Title: Somatostatin interneurons control a key component of mismatch negativity in the mouse visual cortex

Authors: Jordan P. Hamm[1*] and Rafael Yuste[1]

Supplemental Figures:

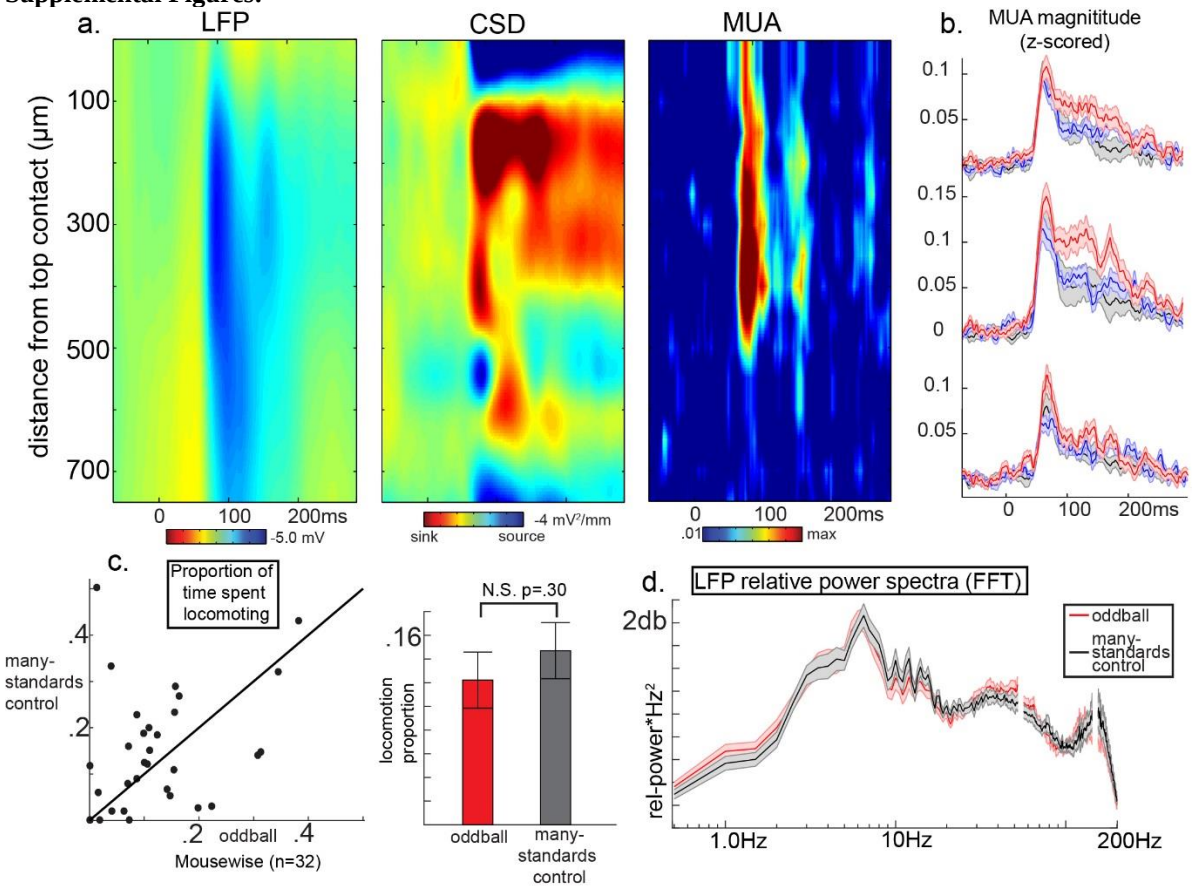

Figure S1. Laminar analysis and equivalent arousal between runs. Related to figure 1. Multielectrode recordings of local field potentials and multiunit activity from a cortical column. a) Interpolated maps of a grating (control) stimulus-evoked response in V1 from a single mouse confirm that a mid-depth (approx. 400um from top contact, approximately localized at the surface) contact displays the largest LFP peak (left), early current sink (middle), and early multiunit "spiking" response (right). These characteristics were used to select and score layer specific multiunit activity, which (b) help corroborate the 2P-Ca2+ evidence of SSA and deviance detection in layer 2/3 (and layer 4) spiking outputs (red=response to deviant; blue=redundant; black=control). c) Locomotion varied across mice but did not differ between typical oddball (redundant and deviant) and "many standards" control runs. d) Relative LFP power spectra (log-scaled with 60 and 180hz line noise removed; averaged across consecutives 2sec bins without locomotion) did not significantly differ for any frequency band measured (all paired t-tests p>.20) and did not show a low to high shift indicative of arousal. Thus equivalent locomotion probability ($F(31)=1.1$, $p>.05$) and LFP power spectra between the "oddball" and "many standards control" runs (all frequency bands $p>.05$, 0.5-200Hz;) indicated that no difference in cortical or physiological arousal could easily explain our effects (Vinck et al., 2015). Error bars reflect within subject standard error across mice.

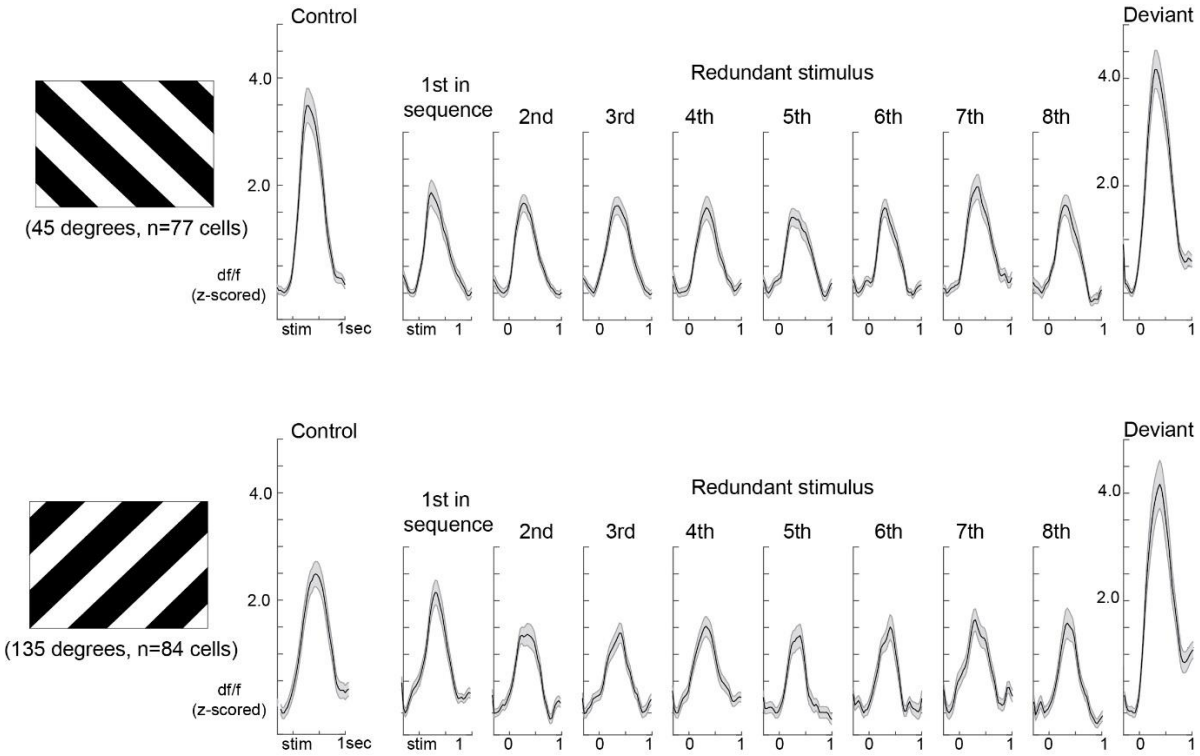

Figure. S2. Single neuron responses sorted by redundant order. Related to figure 1,3. Average 2P-Ca^{2+} responses of neurons (n=160; 18.9% of total) showing average responses (0-1second) of greater than 1.67 standard deviation above prestimulus baseline (i.e. one-tailed significance cutoff) to control, redundant, or deviant stimuli. This proportion is well in line with the fact that, among the 40-50% of neurons in mouse V1 which typically show a reliable response to grating stimuli (Marshel et al., 2011), most show an orientation preference with an average tuning width of 20-degrees (Niell and Stryker, 2010). Responses to redundant stimuli are sorted as a function of their order in "oddball" sequence (1^{st}, 2^{nd}, 3^{rd}, etc. redundant stimulus since last "deviant") and preferred stimulus (45/135 degrees). Only one neuron showed significant responses to both stimuli. Error bars reflect within subject standard error across cells.

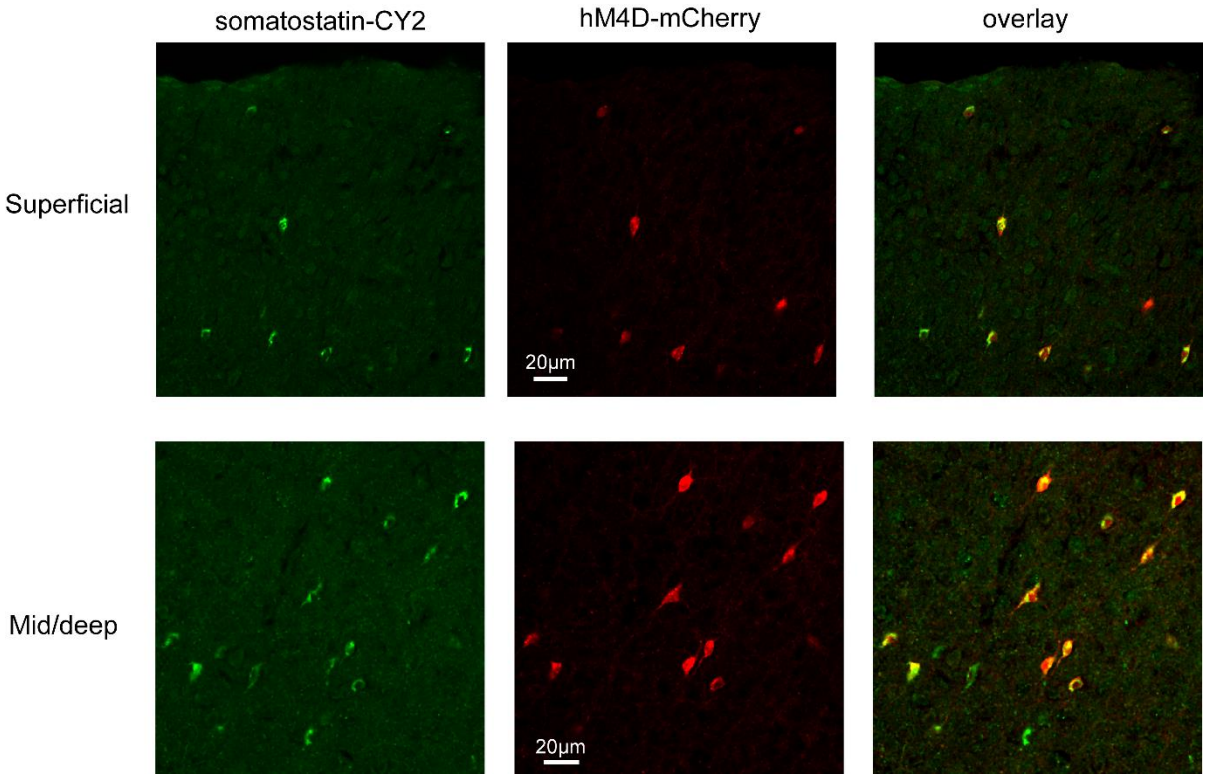

.

Figure S3. Immunohistochemistry. Related to figure 2. Immunohistochemical staining of Somatostatin (with CY2) coexpressing with hM4D-mCherry construct. Mid/deep section taken from 300 micrometer depth (top of image).

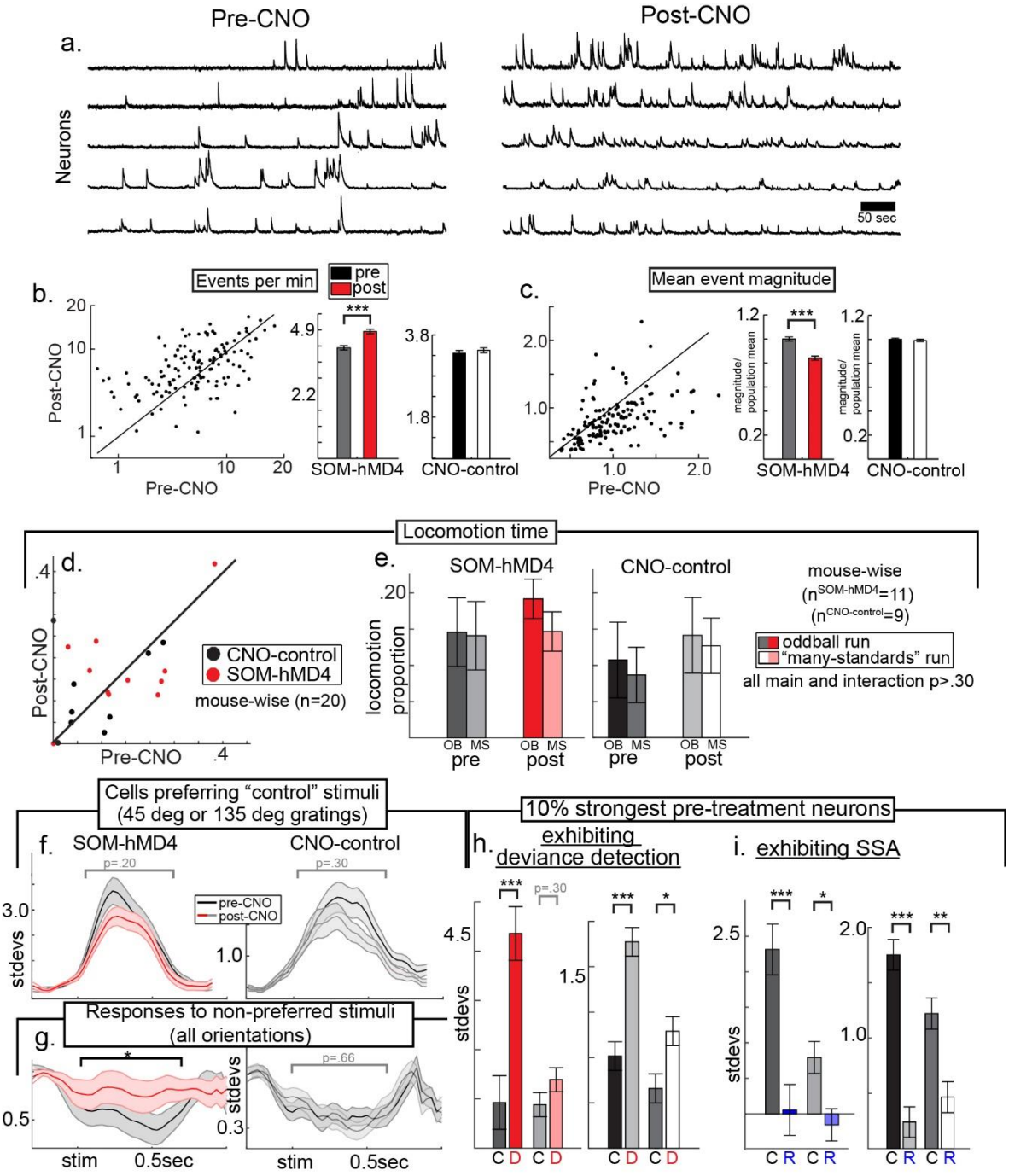

Figure S4. Increase in spontaneous activity after SOM suppression. Related to figure 3. hM4D expression in SOMs lead disinhibits local neurons by (a) increasing the frequency of smaller amplitude calcium transients (putative bursting episodes). (b,c) Quantifying the number of events per minute and the average peak of events demonstrates a significant increase in the former (GROUPxTREATMENT $F(1,133)=15.05$, $p<.001$; one outlier excluded) and decrease in the latter measure (GROUPxTREATMENT $F(1,134)= 27.06$, $p<.001$), no change in CNO-injected control animals (scatterplots and statistics computed on single neurons). One-way ANOVAs ***=p<.001. (d) Neither CNO-treatment alone nor SOM-suppression altered locomotion (proportion of 5-second blocks with treadmill movement), (e) regardless of whether mice were viewing the oddball (only deviants and redundatnds) or multiple grating stimulus orientations in the "many-standards" run (TREATMENT $F(1,18)= 1.68$, $p=.21$; GROUP $F(1,18)= 2.19$, $p=.16$; GROUPxTREATMENT $F(1,18)= .02$, $p=.88$). (f) Average responses (first

500ms post-stim) across all significantly active neurons (i.e. responses to controls greater than 1.67 stdevs above baseline) were not significantly changed by SOM-suppression (repeated measures ANOVA; F(1, 65)=1.66, p=.20) or CNO-control (F(1, 41)=1.08, p=.30) , though cells in both conditions showed nominally weaker responses. (g) Responses to non-preferred orientations decreased below baseline response rates (1 sec pre-stim), and this decrease was diminished at a trend level after SOM-suppression (all matched neurons regardless of preference, $F(1,90)=3.24$, p=.07) but not CNO-control ($F(1,168)=0.08$, p=.77). (h,i) Comparisons of the top 10% of cells showing the strongest deviance detection or SSA (n=30 cno-control, n=14 SOM-hMD4) using unnormalized values matched the pattern of effects seen using magnitude normalized values in figure 3. *=p<.05, **=p<.01, ***p<.001. Error bars reflect within subject standard error across cells (Loftus, 1994).

Supplemental Experimental Procedures.

Animals, Surgery, and Training. For virus injection, mice were anesthetized with isoflurane (initially 3% (partial pressure in air) and reduced to 1-2%). A small window was made through the skull above left V1 using a dental drill (coordinates from lambda: X=-2500, Y=200 μm) taking care not to pierce the dura mater. A glass capillary pulled to a sharp micropipette was advanced with the stereotaxic instrument, and 75ul solution of 1:1 diluted AAV1/Syn:GCaMP6s/f (obtained from the University of Pennsylvania Vector Core; n=20) or a 3:7 mixture of AAV1/Syn:GCaMP6s/f and AAV5hsynDIOhM4D(Gi)mCherry (UNC vector core; n=11 SOM-cre mice) was injected into putative layer 2/3 over a 5 min period at a depth of 200-300 μm from the pial surface using a UMP3 microsyringe pump (World Precision Instruments).

Approximately 2-3 weeks after virus injection, mice were anesthetized with isoflurane and a titanium head plate was attached to the skull centered on the virus injection site using dental cement. Mice were allowed to recover for at least 5 days in their home cage. In this time, mice were given analgesics (5mg/kg carprofen I.P.) and accustomed to experimenter handling, including brief head-restraint periods, until mice showed non-stressed behavior, which usually began on the second day. During training sessions and prior to the first imaging session, mice viewed moving square-wave gratings for stimulus habituation.

Locomotion was recorded with an infared LED/photodarlington pair (Honeywell S&C HOA1877-003), which consists of a small c-shaped device positioned at the edge of the rotating wheel (striped with black tape) connected to the acquisition computer as an analogue input. Five second bins including photodarlington deflections were scored as "locomotion" periods for trial exclusion and for quantifying the proportion of each run the animal spent running. Oddball and "many-standards" runs were separate.

The thin skull preparation prevents exposure of the cortex and meninges (Yang et al., 2010).

Visual Stimulation. The timing and identity of gratings played in MATLAB were synchronized with image acquisition by outputting an analogue voltage trigger synchronized with stimulus onset and offset and recorded with the imaging computer using Prairie View 5.2. The timing between actual stimulus onset and recorded voltage traces in Prairie View or Plexon software was confirmed beforehand using a photodiode sensor with a reverse biased voltage output recorded by the software in tandem with the MATLAB output triggers.

LFP spectral analysis: In order to test whether LFP indices of cortical arousal differed between "oddball" and "many standards" runs (relative high to low power, (Vinck et al., 2015)), LFP data from the peak sensor were segmented into 2-second bins (excluding trials with locomotion and excessive signal), multiplied by a hanning window, and transformed into power spectra by squaring the absolute value of a fast-fourier transformation (Hamm et al., 2012a). Relative power for each mouse was computed by dividing by the average power across all frequencies (excluding 60 and 180hz bands). For plotting simplicity, power was multiplied by squared-Hz for each frequency to flatten the spectra (i.e. remove the 1/f component), and the Hz axis was log-scaled.

Multielectrode analyses: Multiunit activity (MUA) was sampled at 40kHz, digitally filtered (300–5000 Hz; bandpass least squares FIR), rectified, and then downsampled to 1 kHz. The result was low-pass filtered at 100Hz (least squares FIR) to estimate the local population spiking envelope. Putative laminar subregions (3 channels) were defined based on CSD demarcations previously published and histologically verified in mouse V1(Kozai et al., 2015) for each mouse separately based on average CSD plots. In general, grating evoked averages suggested a laminar distribution of activation in response to grating stimuli, with a current sink beginning in layer 4 with corresponding, sustained sources in layer 2/3 and 5. Furthermore, our putative "granular" or middle layer corresponded to the maximum negativity of initial dip in the LFP and, when available, robust early multiunit activity (suggesting population spiking). Average CSD waveforms were again averaged over stimulus orientations since waveforms did not show robust differences, an expected effect given i) the lack of orientation columns in mouse V1 (Niell and Stryker, 2008) and ii) previous LFP recordings in mouse V1(Land et al., 2013). For analyzing stimulus evoked changes in spectral power, We converted single trial LFP traces from putative granular layers (the location of the strongest LFP response; Fig. S1) to time/frequency power spectra using a modified-morlet wavelet approach (4-120Hz; 2Hz steps, 1-14 cycles, 5ms steps from -50 to 450ms poststim) and subsequently averaged across trials and within conditions (fig. 4a). We carried out a principal components analysis on spectra from all conditions and mice to extract 4 distinct frequency bands (based on scree; theta/alpha: 4-12Hz; Beta: 14-32Hz; low-gamma: 34-60; high-gamma: 62-120Hz). This approach was previously optimized in human EEG studies of schizophrenia (Hamm et al., 2012b, 2014).

Image Analysis. Imaging datasets were scored similarly to previous reports(Carrillo-Reid et al., 2015; Chen et al., 2013). The raw images were processed to correct translational brain motion artifacts using an in house plugin named "Moco" for ImageJ (Dubbs et al., 2016; Schneider et al., 2012). Then, cell regions of interest (ROIs) were detected semi-automatically for each imaging session and individually confirmed as follows. Mean, standard

deviation, and std×skewness projections (pixel-wise) were calculated across all imaging frames (roughly 14000-25000) and plotted for reference. Then, rectangular sections were selected around the apparent cell bodies using a GUI created in MATLAB. A principal components analysis (PCA) was computed on the pixels contained within the sections, and the pixels with weights at least 80% of the maximum of the first PCA component were defined as the ROI and spatially plotted along with the florescence trace averaged across these pixels. Cells with no apparent calcium transients were excluded from further analysis at this step. Florescence of active cells was then calculated as the average across all pixels within this ROI minus the average of the pixels just outside the selected rectangle, termed the "halo", which excluded pixels from nearby cell bodies. This subtraction removed background contamination from neuropil and nearby cells. Completing this step ensures maximal correspondence between florescence and actual cell spiking(Chen et al., 2013). The remaining traces were then filtered with a 1-second *lowess* envelope(Masamizu et al., 2014), a regression based smoothing approach which is tolerant of sharply changing baseline values. Finally, the discrete first derivative was scored as delta-f (within cell/single cell comparisons). A 2-10 second baseline window was manually selected for each which contained no apparent calcium transients(Chen et al., 2013). The mean and standard deviation was calculated on the delta-f values in this window for each cell for the whole experiment which was used to i) compute a z-scored delta-f for visualizing and combining activity across cells and ii) determine activation thresholds described below. A minority of mice expressed GCaMP6f (5; 3 SOM-cre) while the rest expressed GCaMP6s. While 6f shows faster decay times and 6s may be slightly more sensitive to single action potentials, we observed evidence for SSA and deviance detection regardless of the indicator used. It is further unlikely that this variability meaningfully altered our conclusions since i) we focused on only the initial rise of transients, and ii) all statistical comparisons were computed within-cell.

Pharmacogenetic suppression of interneurons. Since SOMs show significant spontaneous activity in awake mice (Gentet et al., 2012), whether this manipulation resulted in an expected disinhibition of "ongoing" or baseline activity levels (Zhu et al., 2015) was tested (Fig. S4). The dose of CNO employed was 12 mg/kg, which was within the range of previously reported doses (Perova et al., 2015; Pina et al., 2015; Roth, 2016; Stachniak et al., 2014).

Supplemental Statistical Procedures.

Effect of SOM suppression on baseline activity rates: using metrics computed on baseline periods described above, events were automatically marked as timeframes with delta-f values which exceeded 3.1 stdevs ($p<.001$). The average event maximum and event frequency were then quantified for each cell and condition. Event rates were log-normalized. Event sizes were normalized within each mouse using the pre-treatment within-mouse. These normalization steps did not impact the significance of key effects. For each measure, 2-by-2 mixed ANOVA on individual cells with GROUP (CNO-control; SOM-hM4D) as the between subject variable and TREATMENT (pre/post) as the within subject variable was computed. One-way repeated measures ANOVAs within groups were used to describe interaction effects.

Effect of SOM suppression experimental time spent locomoting: This was assessed with a 2-by-2 mixed ANOVA on with GROUP (CNO-control; SOM-hM4D) as the between subject variable and TREATMENT (pre/post) as the within subject variable. No significant interaction was found.

For comparing the relative LFP power spectrum between the oddball and many standards runs, paired t-tests were computed for each frequency from .5-200Hz (in 0.5 hz steps). No significant effects were found.

Immunohistochemistry. Two SOM-cre mice (p40-50) were injected as described above with AAV5hsynDIOhM4D(Gi)mCherry only and sacrificed for immunostaining 3 weeks later. Mice were anesthetized and perfused transcardially with 4% paraformaldehyde in 0.1M phosphate buffer, pH 7.4. Slices were post-fixed in 4% paraformaldehyde at 4C, and then immersed in 30% sucrose solution for 48 hours at 4C. A vibratome (Leica VT1000s) was used to cut 40-µm thick coronal sections from visual cortex. Sections were blocked in a 1% Bovine serum albumin, 0.5% Triton solution for 1.5 hr at room temperature, then incubated 48hrs with primary antibodies: polyclonal rabbit anti-somatostatin (1:100, Santa Cruz) in 1% Bovine serum albumin and 0.5% Triton. Subsequently, sections were incubated with donkey anti-rabbit CY2 (1: 200; Jackson ImmunoResearch) and mounted. Images from the surface to 700 micrometers in depth were acquired using 40X oil immersion objective with a confocal microscope (Zeiss 700 LSM). Scans were collected in sequential mode with 488/512 excitation/emission filter (somatostatin) and 560/605 (mCherry) and later merged.

Supplemental References:

Carrillo-Reid, L., Miller, J.-E.K., Hamm, J.P., Jackson, J., and Yuste, R. (2015). Endogenous sequential cortical activity evoked by visual stimuli. J. Neurosci. *35*, 8813–8828.

Chen, T.-W., Wardill, T.J., Sun, Y., Pulver, S.R., Renninger, S.L., Baohan, A., Schreiter, E.R., Kerr, R.A., Orger, M.B., Jayaraman, V., et al. (2013). Ultrasensitive fluorescent proteins for imaging neuronal activity. Nature *499*,

295–300.
Dubbs, A., Guevara, J., and Yuste, R. (2016). moco: Fast Motion Correction for Calcium Imaging. Front. Neuroinform. *10*, 6.
Gentet, L.J., Kremer, Y., Taniguchi, H., Huang, Z.J., Staiger, J.F., and Petersen, C.C.H. (2012). Unique functional properties of somatostatin-expressing GABAergic neurons in mouse barrel cortex. Nat. Neurosci. *15*, 607–612.
Hamm, J.P., Gilmore, C.S., and Clementz, B.A. (2012a). Augmented gamma band auditory steady-state responses: Support for NMDA hypofunction in schizophrenia. Schizophr. Res. *138*, 1–7.
Hamm, J.P., Ethridge, L.E., Shapiro, J.R., Stevens, M.C., Boutros, N.N., Summerfelt, A.T., Keshavan, M.S., Sweeney, J.A., Pearlson, G., Tamminga, C.A., et al. (2012b). Spatiotemporal and frequency domain analysis of auditory paired stimuli processing in schizophrenia and bipolar disorder with psychosis. Psychophysiology *49*, 522–530.
Hamm, J.P., Ethridge, L.E., Boutros, N.N., Summerfelt, A.T., Keshavan, M.S., Sweeney, J.A., Pearlson, G., Tamminga, C.A., and Clementz, B.A. (2014). Diagnostic Specificity and Familiality of Early versus Late Evoked Potentials to Auditory Paired-Stimuli across the Schizophrenia-Bipolar Psychosis Spectrum. Psychophysiology.
Kozai, T.D.Y., Du, Z., Gugel, Z. V, Smith, M.A., Chase, S.M., Bodily, L.M., Caparosa, E.M., Friedlander, R.M., and Cui, X.T. (2015). Comprehensive chronic laminar single-unit, multi-unit, and local field potential recording performance with planar single shank electrode arrays. J. Neurosci. Methods *242*, 15–40.
Land, R., Engler, G., Kral, A., and Engel, A.K. (2013). Response properties of local field potentials and multiunit activity in the mouse visual cortex. Neuroscience *254*, 141–151.
Loftus, G.R. (1994). Using confidence intervals in within-subject designs. Psychon. Bull. Rev. *1*, 476–490.
Marshel, J.H., Garrett, M.E., Nauhaus, I., and Callaway, E.M. (2011). Functional specialization of seven mouse visual cortical areas. Neuron *72*, 1040–1054.
Masamizu, Y., Tanaka, Y.R., Tanaka, Y.H., Hira, R., Ohkubo, F., Kitamura, K., Isomura, Y., Okada, T., and Matsuzaki, M. (2014). Two distinct layer-specific dynamics of cortical ensembles during learning of a motor task. Nat. Neurosci. *17*, 987–994.
Niell, C.M., and Stryker, M.P. (2008). Highly selective receptive fields in mouse visual cortex. J. Neurosci. *28*, 7520–7536.
Niell, C.M., and Stryker, M.P. (2010). Modulation of visual responses by behavioral state in mouse visual cortex. Neuron *65*, 472–479.
Perova, Z., Delevich, K., and Li, B. (2015). Depression of Excitatory Synapses onto Parvalbumin Interneurons in the Medial Prefrontal Cortex in Susceptibility to Stress. J. Neurosci. *35*, 3201–3206.
Pina, M.M., Young, E.A., Ryabinin, A.E., and Cunningham, C.L. (2015). The Bed Nucleus of the Stria Terminalis Regulates Ethanol-Seeking Behavior in Mice. Neuropharmacology *99*, 627–638.
Roth, B.L. (2016). DREADDs for Neuroscientists. Neuron *89*, 683–694.
Schneider, C.A., Rasband, W.S., and Eliceiri, K.W. (2012). NIH Image to ImageJ: 25 years of image analysis. Nat. Methods *9*, 671–675.
Stachniak, T.J., Ghosh, A., and Sternson, S.M. (2014). Chemogenetic synaptic silencing of neural circuits localizes a hypothalamus→midbrain pathway for feeding behavior. Neuron *82*, 797–808.
Vinck, M., Batista-Brito, R., Knoblich, U., and Cardin, J.A. (2015). Arousal and Locomotion Make Distinct Contributions to Cortical Activity Patterns and Visual Encoding. Neuron *86*, 740–754.
Yang, G., Pan, F., Parkhurst, C.N., Grutzendler, J., and Gan, W.-B. (2010). Thinned-skull cranial window technique for long-term imaging of the cortex in live mice. Nat. Protoc. *5*, 201–208.
Zhu, Y., Qiao, W., Liu, K., Zhong, H., and Yao, H. (2015). Control of response reliability by parvalbumin-expressing interneurons in visual cortex. Nat. Commun. *6*, 6802.